Redox Biology 17 (2018) 16–24

Contents lists available at ScienceDirect

Redox Biology

journal homepage: www.elsevier.com/locate/redox

Research Paper

IDH2 deficiency accelerates skin pigmentation in mice via enhancing melanogenesis

Jung Hyun Park[a], Hyeong Jun Ku[b], Jin Hyup Lee[a,*], Jeen-Woo Park[b,*]

[a] Department of Food and Biotechnology, Korea University, Sejong, Republic of Korea
[b] School of Life Sciences and Biotechnology, BK21 Plus KNU Creative BioResearch Group, College of Natural Sciences, Kyungpook National University, Taegu, Republic of Korea

ARTICLE INFO

Keywords:
Melanogenesis
α-MSH
IDH2
Mitochondria
Mito-TEMPO

ABSTRACT

Melanogenesis is a complex biosynthetic pathway regulated by multiple agents, which are involved in the production, transport, and release of melanin. Melanin has diverse roles, including determination of visible skin color and photoprotection. Studies indicate that melanin synthesis is tightly linked to the interaction between melanocytes and keratinocytes. α-melanocyte-stimulating hormone (α-MSH) is known as a trigger that enhances melanin biosynthesis in melanocytes through paracrine effects. Accumulated reactive oxygen species (ROS) in skin affects both keratinocytes and melanocytes by causing DNA damage, which eventually leads to the stimulation of α-MSH production. Mitochondria are one of the main sources of ROS in the skin and play a central role in modulating redox-dependent cellular processes such as metabolism and apoptosis. Therefore, mitochondrial dysfunction may serve as a key for the pathogenesis of skin melanogenesis. Mitochondrial $NADP^+$-dependent isocitrate dehydrogenase (IDH2) is a key enzyme that regulates mitochondrial redox balance and reduces oxidative stress-induced cell injury through the generation of NADPH. Downregulation of *IDH2* expression resulted in an increase in oxidative DNA damage in mice skin through ROS-dependent ATM-mediated p53 signaling. IDH2 deficiency also promoted pigmentation on the dorsal skin of mice, as evident from the elevated levels of melanin synthesis markers. Furthermore, pretreatment with mitochondria-targeted antioxidant mito-TEMPO alleviated oxidative DNA damage and melanogenesis induced by IDH2 deficiency both *in vitro* and *in vivo*. Together, our findings highlight the role of IDH2 in skin melanogenesis in association with mitochondrial ROS and suggest unique therapeutic strategies for the prevention of skin pigmentation.

1. Introduction

Melanogenesis, the process of melanin pigment production, is a complex biosynthetic pathway regulated by multiple agents, which are involved in the production, transport, and release of melanin [1]. Melanin has diverse roles and functions in various organisms; for instance, the visible skin color is determined by the distribution of melanin in the skin epidermis [2]. Numerous studies have indicated melanin as an important photo-protective factor involved in the absorption and reflection of UV irradiation [3]. In addition, melanin functions as an antioxidant by scavenging oxidative free radicals [4].

Melanogenesis is tightly linked to the interaction between melanocytes and keratinocytes [5]. Melanogenesis in melanocytes is under the control of secreted factors from neighboring keratinocytes [6]. Keratinocytes produce and secrete factors such as α-melanocyte-stimulating factor (α-MSH), which regulates and stimulates the epidermal melanogenesis of melanocytes [7–10]. The stimulated melanosomes in melanocytes synthesize melanin and induce the transfer of melanin from melanocytes to keratinocytes [5]. The microphthalmia-transcription factor (MITF) is the most important factor that regulates the differentiation and development of melanocytes in melanogenesis [11]. MITF controls the expression of melanocyte-specific proteins such as tyrosinase and tyrosinase-related protein 1 and 2 (TRP1 and TRP2), which regulate the synthesis of melanin [12,13].

Reactive oxygen species (ROS) are shown to play a major role in skin melanogenesis [14]. Skin is continuously exposed to harmful environmental sources such as UV irradiation, resulting in the generation of ROS, which consequently cause DNA damage in both keratinocytes and melanocytes [15–17]. ROS may be transported from keratinocytes to melanocytes and affect several biosynthetic processes in melanocytes [18]. An increase in ROS level was observed during melanogenesis [15], and treatment with antioxidants was shown to inhibit skin pigmentation [19].

In human skin, mitochondria are one of the main sources of ROS

* Corresponding authors.
E-mail addresses: jinhyuplee@korea.ac.kr (J.H. Lee), parkjw@knu.ac.kr (J.-W. Park).

https://doi.org/10.1016/j.redox.2018.04.008
Received 9 February 2018; Received in revised form 3 April 2018; Accepted 5 April 2018
Available online 06 April 2018

[20] and are major organelles involved in the regulation of cellular redox status [21]. Accumulating evidence indicates that mitochondria are sensitive to oxidative stress, as these are the major sites of ROS generation and exhibit limited function to eliminate oxidants [22]. Excess ROS production induces mitochondrial dysfunction and impairs oxidative stress balance, which are believed to play a crucial role in the pathogenesis of metabolic diseases [23–25]. Numerous studies have indicated that mitochondria play a role in processes such as melanogenesis [26]. The complex V of mitochondria has been identified as the modulator of skin pigmentation [27]. In addition, mitochondria were shown to regulate the biogenesis of melanosomes [28].

Mitochondrial isocitrate dehydrogenase 2 (IDH2), a subtype of isocitrate dehydrogenases, is located in mitochondria and known to generate NADPH [29]. IDH2 plays the role of an antioxidant protein against ROS by converting $NADP^+$ to NADPH, which promotes the regeneration of reduced glutathione (GSH) from oxidized glutathione (GSSG) [30]. The role of IDH2 is very important in the pathogenesis of some metabolic diseases, and the deficiency of IDH2 results in various ROS-mediated metabolic syndromes [31,32]. Therefore, IDH2 may play an important role in melanogenesis [33].

In the present study, we examined the role of IDH2 in skin melanogenesis by using both *in vitro* and *in vivo* models. We found that IDH2 deficiency results in the generation of ROS in the mitochondria and secretion of α-MSH in keratinocytes, eventually leading to an increase in melanin production in melanocytes. We believe that the knowledge of the involvement of mitochondria in skin melanogenesis may be useful to design potential therapeutic strategies for skin disorders.

2. Materials and methods

2.1. Materials

Gil No. 3 hematoxylin and eosin Y (H&E) solution, xylenol orange, L-DOPA, and mito-TEMPO were obtained from Sigma-Aldrich (St. Louis, MO). The Masson-Fontana staining kit was purchased from BioGnost (Zagreb, Croatia). JC-1 mitochondrial membrane potential probe was supplied by Thermo Fischer Scientific (Waltham, MA), and 2′,7′-dichloro-fluorescein diacetate (DCFH-DA) by Molecular Probes (Eugene, OR). MitoSOX Red was procured from Invitrogen (Eugene, OR), and the cAMP assay kit from Abcam (Cambridge, MA). The mouse α-MSH ELISA kit was obtained from Abbkine (Wuhan, China). The antibodies used in this study were acquired from Cell Signaling (Beverly, MA), Abcam (Cambridge, MA), Santa Cruz Biotechnology (Santa Cruz, CA), Virogen (Watertown, MA), Biorbyt (Cambridge, UK), Calbiochem (San Diego, CA), and AbFrontier (Seoul, Korea).

2.2. Cell culture

The murine keratinocyte cell line JB6 CI 41-5a was obtained from the American Type Culture Collection (Manassas, VA). Cells were cultured in Minimum essential medium (Eagle) containing 2 mM L-glutamine, 1.5 g/L sodium bicarbonate, 0.1 mM non-essential amino acids, 1.0 mM sodium pyruvate, 5% fetal calf serum (FBS), and 1% penicillin/streptomycin in a humidified atmosphere of 5% CO_2 at 37 °C. B16F10 mouse melanoma cells were purchased from the Korean Cell Line Bank (Seoul, Korea). Cells were cultured with growth medium as previously described [31]. For the conditioned medium, JB6 cells transfected with *IDH2* shRNA and non-target shRNA were cultured under conditions previously described for 48 h [34]. After 48 h, the supernatant was collected and used as the conditioned medium. B16F10 cells were cultured with the conditioned medium for 48 h. The conditioned medium was changed every day. For mito-TEMPO treatment, JB6 cells transfected with *IDH2* shRNA were cultured with the described condition for 24 h. After 24 h, cells were treated with 200 nM of mito-TEMPO for 24 h. Following incubation, the supernatant was collected and used as the conditioned medium. B16F10 cells were cultured in the presence of conditioned medium and mito-TEMPO-treated medium for 48 h. The conditioned medium was changed every day.

2.3. IDH2 shRNA knockdown

IDH2 short-hairpin RNA (shRNA) and non-target shRNA MISSION® lentiviral transduction particles were purchased from Sigma. JB6 cells were transduced with hexadimethrine bromide at a final concentration of 8 μg/mL, as per the manufacturer's protocol. Transduced cells were selected as single colonies in medium containing 5 μg/mL puromycin (Clontech, Mountain View, CA) and maintained in medium containing 1 μg/mL puromycin.

2.4. Animal protocols

All animal experiments were reviewed and approved by the Kyungpook National University Institutional Animal Care and Use Committee. We used 10–12 weeks old male C57BL/6 mice. The mice had the following genotypes: wild-type (WT, $IDH2^{+/+}$) or knockout (KO, $IDH2^{-/-}$). Mice were identified by polymerase chain reaction (PCR) genotyping, as previously described [31]. Animals were housed at a consistent 22 °C temperature and 12 h of light/dark cycle; the dorsal skin was shaved with a trimmer, followed by animal euthanization. For mito-TEMPO experiments, mice received a daily injection of mito-TEMPO (0.7 mg/kg, intraperitoneal) starting at week 6 for 30 days [35].

2.5. Immunoblot analysis

Total protein extracts were resolved by sodium dodecyl sulfate polyacrylamide gel electrophoresis (SDS-PAGE) and the protein bands were transferred onto nitrocellulose membranes and probed with appropriate primary antibodies. Proteins were visualized using horseradish peroxidase-labeled anti-rabbit IgG and an enhanced chemiluminescence detection kit (Amersham Pharmacia Biotech, Buckinghamshire, UK). Protein expression was analyzed using Image J software.

2.6. Measurement of melanin content

B16F10 cells were incubated with the conditioned media for 2 days. After incubation, cells were collected, washed twice with ice-cold phosphate-buffered saline (PBS), and centrifuged at 13,000 ×*g* for 15 min. Pellets were dissolved in 1 N sodium hydroxide (NaOH) containing 10% dimethyl sulfoxide (DMSO) for 30 min at 56 °C. Cell lysates were placed in a 96-well microplate and the absorbance measured at 405 nm wavelength. The mice dorsal skin samples were homogenized and centrifuged at 13,000 ×*g* for 15 min. The supernatants were collected. Skin tissue lysate was dissolved in 1 N NaOH and the procedure was performed, as previously described. Relative melanin production was calculated by normalizing the absorbance values with the protein concentrations (absorbance/μg protein).

2.7. Measurement of tyrosinase activity

B16F10 cells were incubated with conditioned media for 2 days. Cell were washed with ice-cold PBS and lysed with PBS containing 1% Triton X-100. After centrifugation at 13,000 ×*g* for 15 min, the supernatant was collected. The amount of cell lysate was adjusted with lysis buffer as protein concentration. A total of 50 μL cell supernatant and 10 μL of 2 mg/mL L-DOPA were added in a well of a 96-well plate. After incubation at 37 °C for 1 h, absorbance values were recorded at 475 nm wavelength. Skin tissue lysates were prepared, as previously described.

2.8. Assessment of cellular redox status

The concentration of intracellular hydrogen peroxide was measured using an oxidant-sensitive fluorescent probe, DCFH-DA. After incubation, cells were treated with 10 μM DCFH-DA for 30 min at 37 °C and ROS levels were analyzed using Zeiss Axiovert 200 inverted microscope.

2.9. Mitochondrial membrane potential and ROS

To evaluate the mitochondrial redox status, JC-1 fluorescent probe was used for the detection of mitochondrial membrane potential. Cells were washed with PBS and incubated with 5 μM JC-1 for 20 min at 37 °C. The ratio of the green and red fluorescent intensities was used as an indicator of mitochondrial membrane potential [36]. The mitochondrial ROS level was measured using MitoSOX Red fluorescent dye. Cells were washed with PBS and incubated with 10 μM MitoSOX Red for 20 min at 37 °C. To quantify ROS production in dorsal skin tissue, paraformaldehyde-fixed sections (5 μM) were incubated with 10 μM MitoSOX Red for 15 min at room temperature in the dark. Each fluorescent image was evaluated using Zeiss Axiovert 200 inverted microscope.

2.10. Histological analysis and immunostaining

Cells were fixed with 3% formaldehyde in PBS for 15 min at room temperature and gently washed twice with PBS. Methanol permeabilization step was performed with 100% ice-cold methanol at − 20 °C for 10 min. After fixation, the immunostaining step was performed, as previously described [31]. For animal study, the dorsal skin was fixed in 10% formalin after euthanasia. Samples were dehydrated and subjected to paraffin embedment. The skin was embedded with paraffin and 5 μm sections were sliced. Each slide was subjected to deparaffinization and rehydration phases. Skin sections were sequentially stained with hematoxylin Gill No. 3, bluing solution, and eosin Y by gentle shaking at room temperature to determine skin morphology. Masson-Fontana staining was performed with Masson-Fontana staining kit as per the manufacturer's protocol. Immunohistochemistry was performed on paraffin-embedded dorsal skin sections. Deparaffinized sections were subjected to an antigen-unmasking step. Sections were boiled at 98 °C in 10 mM sodium citrate buffer for 10 min and cooled for 20 min. Immunostaining was performed as previously described [37].

2.11. Statistical analysis

The results are shown as the mean ± standard deviation (SD). Statistical differences among groups were calculated using Student's *t*-test. A value of $p < 0.05$ was regarded as statistically significant.

3. Results and discussion

3.1. Effects of IDH2 downregulation on melanogenesis in JB6 cells

To investigate the role of IDH2 in the activation of the melanogenesis signaling pathway *in vitro*, we used JB6 murine keratinocytes and B16F10 murine melanoma cells. We evaluated the effect of IDH2 with conditioned medium from *IDH2* shRNA-transfected and non-target shRNA-transfected JB6 cells. As shown in Fig. 1A-F, silencing of *IDH2* resulted in an increase in the levels of melanogenesis signals such as α-MSH and pro-opiomelanocortin (POMC), a precursor of α-MSH. The expression level of α-MSH was evaluated with enzyme-linked immunosorbent assay (ELISA) (Fig. 1A) and immunoblot (Fig. 1C) analyses. In addition, we measured the secretion of α-MSH using immunoblot analysis with the conditioned medium from *IDH2* shRNA-transfected and control JB6 cells (Fig. 1B). Furthermore, we assessed the immunofluorescence image for α-MSH in JB6 keratinocytes counterstained with anti-keratin antibody (Fig. 1D). These data indicate that the expression level of α-MSH increased in *IDH2* shRNA-transfected cells. We examined the intracellular expression level of POMC with immunoblot analysis and immunohistochemistry (Fig. 1E and Fig. 1F) and found that the level of POMC increased in *IDH2* shRNA-transfected cells.

To investigate the mechanism underlying the effect of IDH2 knockdown on melanogenesis, we evaluated the phosphorylation and activation of the ATM–Chk2–p53 signaling axis, which plays an important role in responses to various stress conditions such as oxidative stress [38–40]. We observed the phosphorylation level of γ-H2AX, a marker of DNA damage [41]. Previous studies indicate that the phosphorylation of p53 in response to DNA damage results in the induction of α-MSH signaling in keratinocytes [38–40]. As shown in Fig. 1G, an increase in the phosphorylation level of ATM, Chk2, p53, and γ-H2AX was observed in *IDH2* shRNA-transfected cells. This result suggests that the downregulation of IDH2 induces DNA damage in JB6 keratinocytes.

We hypothesized that mitochondrial ROS generation may cause cellular oxidative stress that induces DNA damage, leading to the activation of p53 and generation of POMC. The expressed POMC is eventually broken down into α-MSH [42]. To investigate this hypothesis, we evaluated mitochondrial ROS generation in response IDH2 deficiency. ROS production leads to mitochondrial dysfunction [32]. To confirm the oxidative damage induced by generated ROS, we used 8-OH-dG, a marker of oxidative DNA damage [43], for the quantification of oxidative DNA damage in IDH2-downregulated JB6 cells (Fig. 1H). Furthermore, we investigated whether the attenuation of IDH2 expression results in the induction of cellular ROS production. DCFH-DA fluorescent dye was used to detect the level of hydrogen peroxide (Fig. 1H). Studies have shown that the accumulated mitochondrial ROS disrupts mitochondria membrane potential [44,45]. JC-1 probe, used for the investigation of the mitochondrial membrane potential, indicates healthy and polarized regions in mitochondria with red fluorescence, while depolarized regions are indicated with green fluorescence [36]. We found that the suppression of IDH2 expression resulted in a decrease in the red fluorescence and increase in the green fluorescence from the mitochondrial membrane (Fig. 1H). To probe ROS in mitochondria, mitochondrial ROS-specific fluorescent dye MitoSOX Red was used (Fig. 1H). We detected an increase in the mitochondrial ROS level in *IDH2* shRNA-transfected cells. Thus, the knockdown of IDH2 resulted in the induction of mitochondrial ROS production. The oxidation of sulfonic form of peroxiredoxin (Prx) may serve as a marker of oxidative damage [24]. Immunoblot analysis of Prx-SO_3 levels indicates the increase in the oxidative damage in *IDH2* shRNA-transfected cells as compared to controls (Fig. 1I).

We demonstrated that the suppression of IDH2 expression in JB6 keratinocytes results in the generation and secretion of α-MSH via p53 apoptosis signal pathways. To determine whether the secreted α-MSH exerts any effect on B16F10 cells, we cultured B16F10 cells with JB6 conditioned media from *IDH2* shRNA-transfected JB6 cells. After 48 h incubation, we evaluated the levels of melanogenesis markers. As shown in Fig. 1J, an increase in the melanin content was observed with Masson-Fontana staining. To assess the effects of the knockdown of IDH2 on melanogenesis, we measured the intracellular melanin content (Fig. 1K) and found it to be significantly increased in B16F10 cells incubated with conditioned media from *IDH2* shRNA-transfected JB6 cells. In addition, we determined the expression of melanocyte differentiation markers with immunoblotting. TRP1, TRP2, tyrosinase, and MITF expressions were elevated in B16F10 cells incubated with conditioned media from *IDH2* shRNA-transfected JB6 cells (Fig. 1L). Furthermore, we analyzed the intracellular tyrosinase activity to assess the effect of IDH2 knockdown on melanogenesis mechanism. As shown in Fig. 1M, an increase in the tyrosinase activity was observed in B16F10 cells incubated with conditioned media from *IDH2* shRNA-transfected JB6 cells. The generated α-MSH stimulates melanogenesis via cAMP pathway [46]. Thus, cAMP production may be used as a possible

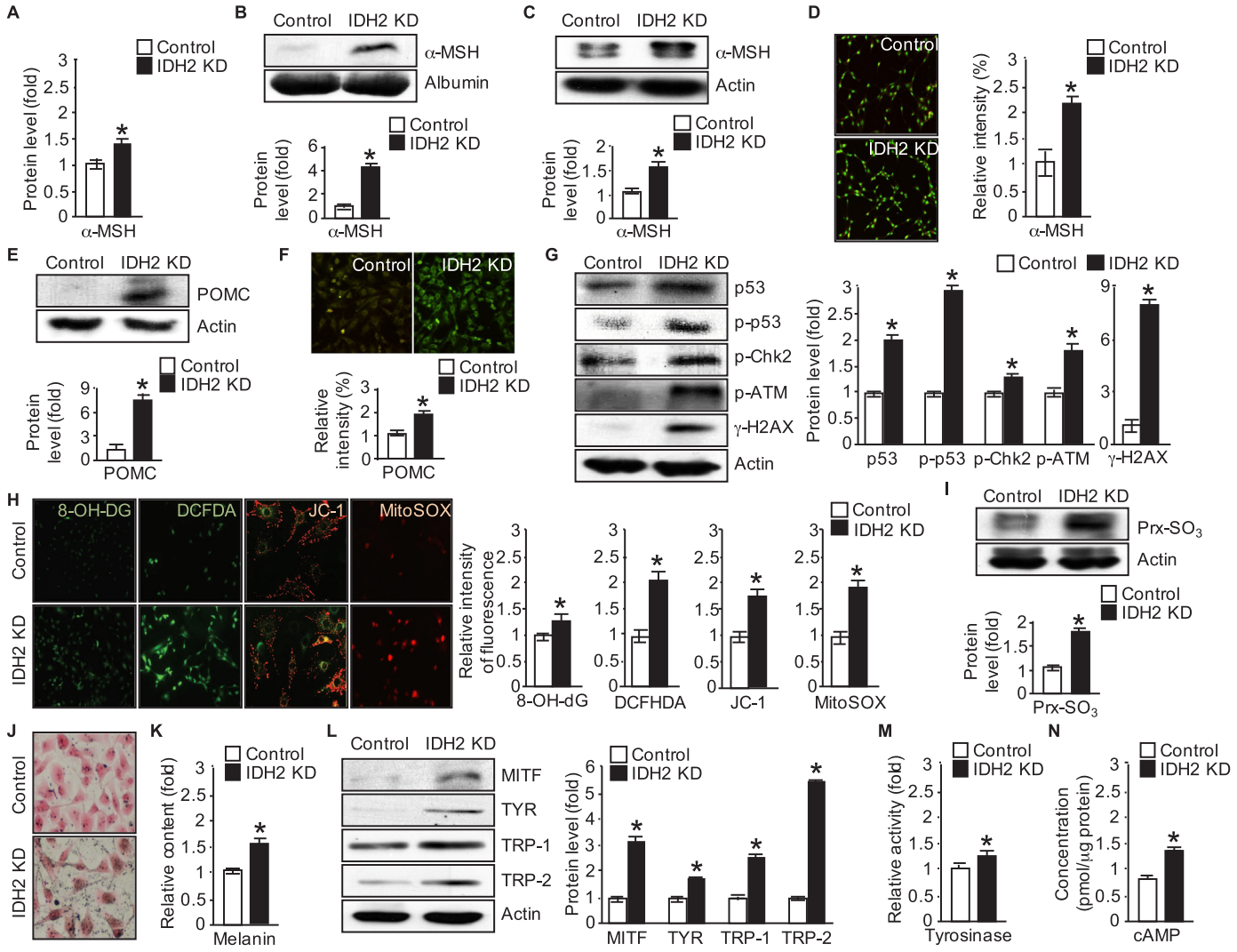

Fig. 1. Effects of IDH2 downregulation on melanogenesis in JB6 cells. (A) Intracellular α-MSH concentration in JB6 keratinocytes measured with α-MSH assay kit. (B) Immunoblot analysis of the secreted α-MSH in JB6-conditioned media. After 48 h of JB6 cultivation, the supernatant was collected and used as the conditioned medium. Media were concentrated and processed for immunoblot analysis. (C) Immunoblot analysis of α-MSH in JB6 keratinocytes. (D) Immunofluorescence image of α-MSH in JB6 keratinocytes. (E) Immunoblot analysis of POMC in JB6 keratinocytes. (F) Immunofluorescence image of POMC in JB6 keratinocytes. (G) Immunoblot analysis of proteins related to ATM-mediated DNA damage signal activation in JB6 keratinocytes. Actin was used as a loading control. The proteins levels were normalized to actin level. (H) Representative immunofluorescence images of 8-OH-dG (green) analysis to measure the oxidative DNA damage. DCFH-DA fluorescence levels for the evaluation of the intracellular hydrogen peroxide level in JB6 keratinocytes after the inhibition of IDH2 expression. Mitochondrial membrane potential (MP) in JB6 keratinocytes was evaluated by measuring JC-1 fluorescence level. The histogram represents the quantification of MP as a ratio of JC-1 (green/red) in different treatment groups. MitoSOX fluorescence level for used for the evaluation of mitochondrial ROS generation in JB6 keratinocytes. All fluorescence images were counterstained with Hoechst 33342 for nuclear morphology. All histograms represent quantification of fluorescence intensity. (I) Immunoblot analysis of Prx-SO_3 levels in JB6 keratinocytes. (J) Masson-Fontana staining for melanin content evaluation in B16F10 cells. Cells were cultured with JB6-conditioned media for 48 h. The medium was changed every day. (K) Intracellular melanin content of B16F10 melanoma cells. Cells were cultured with conditioned media for 48 h. (L) Immunoblot analysis of melanin synthesis markers MITF, tyrosinase, TRP1, and TRP2 in B16F10 melanoma cells. Cells were cultured with conditioned media for 48 h. Actin was used as a loading control. The proteins levels were normalized to actin level. (M) Analysis of tyrosinase activity and cAMP content in B16F10 melanoma cells. Cells were cultured with conditioned media for 48 h. All histograms represent the quantification of fluorescence intensity. In A-N, results are shown as the mean ± SD (n = 3). $*p < 0.05$ versus control cells.

indicator of melanogenesis pathway. We measured the intracellular cAMP level with cAMP assay kit and found an increase in the level of cAMP in B16F10 cells incubated with conditioned media from *IDH2* shRNA-transfected JB6 cells. These data indicate that the knockdown of IDH2 results in the secretion of α-MSH in keratinocytes and the secreted α-MSH induces differentiation and increases melanin synthesis in melanoma cells.

3.2. Mito-TEMPO alleviates the elevated level of melanogenesis by IDH2 downregulation in vitro

Our data showed that the suppression of IDH2 expression resulted in an increase in the cellular and mitochondrial ROS level in JB6 keratinocytes, which eventually led to melanogenesis in B16F10 melanoma cells. To determine whether mitochondrial ROS play a major role in melanogenesis in response to IDH2 knockdown, mito-TEMPO was used. Mito-TEMPO, a novel mitochondria-targeted antioxidant, protects mitochondria from various oxidative stress under diverse pathological processes [47–49]. We treated *IDH2* shRNA-transfected JB6 cells with

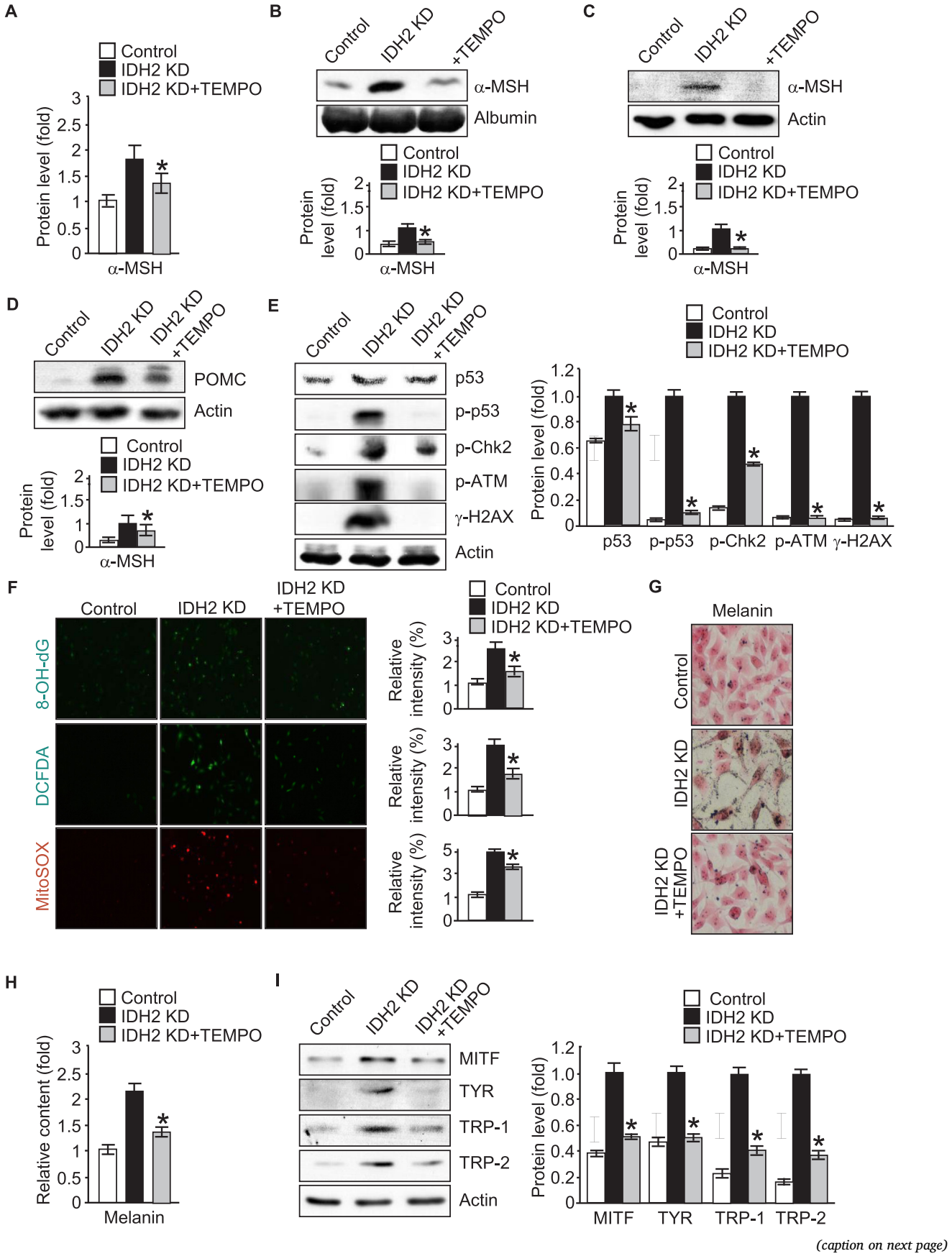

(caption on next page)

Fig. 2. Mito-TEMPO alleviates the increased level of melanogenesis via IDH2 downregulation *in vitro*. JB6 cells were incubated for 24 h after seeding and treated with mito-TEMPO (200 nM) for 24 h. (A) Intracellular α-MSH concentration in JB6 keratinocytes was measured with α-MSH assay kit. (B) Immunoblot analysis of the secreted α-MSH in JB6 conditioned media. Media were concentrated and processed for immunoblot analysis. (C) Immunoblot analysis of α-MSH in JB6 keratinocytes. (D) Immunoblot analysis of POMC in JB6 keratinocytes. (E) Immunoblot analysis of proteins related to ATM-mediated DNA damage signal activation in JB6 keratinocytes. Actin was used as a loading control. The proteins levels were normalized to the actin level. (F) Representative immunofluorescence images of 8-OH-dG (Green) analysis to evaluate the oxidative DNA damage. DCFH-DA fluorescence levels for the evaluation of the intracellular hydrogen peroxide level. Mito-SOX fluorescence level for the evaluation of mitochondrial ROS generation in JB6 keratinocytes. All fluorescence images were counterstained with Hoechst 33342 for nuclear morphology. All histograms represent quantification of fluorescence intensity. (G) Masson-Fontana staining for melanin content evaluation in B16F10 cells. Cells were cultured with JB6 conditioned media for 48 h. For mito-TEMPO-treated conditioned media, JB6 cells seeded for 24 h were treated with 200 nM mito-TEMPO for 24 h. The medium was changed every day. (H) Intracellular melanin contents of B16F10 cultured with conditioned media. (I) Immunoblot analysis of melanin synthesis markers such as MITF, tyrosinase, TRP1, and TRP2 in B16F10 melanoma cells. Cells were cultured with conditioned media for 48 h. Actin was used as a loading control. The proteins levels were normalized to actin level. All histograms represent the quantification of fluorescence intensity. In A-I, results are shown as the mean ± SD (n = 3). $^{*}p < 0.05$ versus IDH2 shRNA-transfected cells.

200 nM of mito-TEMPO for 24 h. For the treatment with conditioned medium, *IDH2* shRNA-transfected JB6 cells were cultured for 48 h as previously described. In addition, cells were treated with 200 nM mito-TEMPO for 24 h. We evaluated the expression level of α-MSH with ELISA (Fig. 2A) and immunoblot analysis (Fig. 2C). We also measured the secretion of α-MSH using immunoblot analysis with conditioned medium from *IDH2* shRNA-treated and control JB6 cells (Fig. 2B). The knockdown of IDH2 resulted in an increase in the expression of α-MSH in JB6 keratinocytes. However, the pretreatment with mito-TEMPO resulted in the reduction in α-MSH expression. As shown in Fig. 2D, the expression level of POMC was detected with immunoblotting and found to be elevated in *IDH2* shRNA-transfected group; however, the pretreatment with mito-TEMPO ameliorated this effect. To investigate whether the effect of mito-TEMPO treatment on DNA damage results in the phosphorylation of p53 and induction of α-MSH expression [50], we performed immunoblot analysis for the detection of the phosphorylation level of the ATM-Chk2-p53 signaling axis and γ-H2AX (Fig. 2E). We found a decrease in the level of p53, phosphorylated p53, Chk2, ATM, and γ-H2AX in mito-TEMPO-treated group. These data indicate that the deficiency of IDH2 induces DNA damage in JB6 keratinocytes, while this effect may be ameliorated following treatment with mito-TEMPO. We measured ROS level and oxidative DNA damage (Fig. 2F). As shown Fig. 2F, the level of mitochondrial ROS, cellular ROS, and oxidative DNA damage was higher in *IDH2* shRNA-transfected group; the pretreatment with mito-TEMPO ameliorated these effects. These results indicate that the treatment with mito-TEMPO attenuates mitochondrial ROS accumulation, leading to the amelioration of oxidative damage in keratinocytes. To determine whether the treatment with mito-TEMPO affects α-MSH secretion by keratinocytes and the consequent effect on B16F10 melanoma cells, we cultured B16F10 cells with conditioned media from *IDH2* shRNA-transfected JB6 cells, including those treated with mito-TEMPO (MT). As shown Fig. 2G, Masson-Fontana staining was used to determine the cellular melanin content. In addition, we measured the cellular melanin content (Fig. 2H) and found that the knockdown of IDH2 resulted in an increase in the cellular melanin content, while pretreatment with mito-TEMPO ameliorated this effect. We used immunoblot analysis to detect the effect of mito-TEMPO on B16F10 melanogenesis (Fig. 2I) and found elevated expression of melanin synthesis markers; this effect was abrogated following treatment with mito-TEMPO. Taken together, the knockdown of IDH2 results in the accumulation of cellular melanin content and increases the expression level of melanin synthesis markers, while the treatment with mito-TEMPO alleviates these effects.

3.3. Effects of IDH2 deficiency on skin melanogenesis of mice

We demonstrated that the knockdown of IDH2 induces melanogenesis pathway by enhancing mitochondrial oxidative stress *in vitro*. To determine the effect of the deficiency of IDH2 on skin pigmentation *in vivo*, C57BL/6 male *IDH2*$^{+/+}$ (WT) and *IDH2*$^{-/-}$ KO mice were used. Briefly, 10–12–week old mice were shaved dorsally with a trimmer and anesthetized. As shown in Fig. 3A, WT mice displayed normal skin, whereas KO mice exhibited noticeable skin pigmentation. The skin pigmentation in KO mice was apparent only after 10–12 weeks, indicating that this phenomenon is senescence-associated. Microscopic examination of H&E-stained sections confirmed the difference between WT and KO mice in terms of the integrity of skin layers and thickness (Fig. 3B). The image indicates that the dorsal skin of KO mice showed thick epidermis layers. Melanin was more distributed in the whole layer of the epidermis, including melanocytes and keratinocytes. As shown in Fig. 3C, Masson-Fontana-stained images showed an increase in the concentration of melanin pigments in KO mice. Furthermore, we investigated the intracellular melanin content (Fig. 3D) and tyrosinase activity (Fig. 3E) to assess the effect of IDH2 deficiency on melanogenesis. This result indicates that the skin of KO mice showed markedly increased melanin content and enhanced tyrosinase activity as compared with WT mice. To determine whether the deficiency of IDH2 affects melanogenesis pathway *in vivo*, immunohistochemistry was used. We determined the expression of melanin synthesis markers in dorsal skin tissues by immunostaining. Immunohistochemistry analysis revealed an increase in the expression level of TRP1, TRP2, tyrosinase, and MITF in skin melanocytes (Fig. 3F). All sections were counterstained with anti-melanoma antibody (red) for pan-melanocytes and Hoechst 33342 (blue) for nuclear morphology. This phenomenon was also observed in immunoblot analysis (Supplementary Fig. 1A). These data indicate that IDH2 deficiency promoted melanogenesis pathways. Immunofluorescence staining for α-MSH and POMC was used to determine the effect of IDH2 deficiency on α-MSH and POMC levels *in vivo* (Fig. 3G). All sections were counterstained with anti-keratin antibody (red) for pan-keratinocytes and Hoechst 33342 (blue) for nuclear morphology. The result indicates that levels of α-MSH and POMC were markedly increased in KO mice as compared with WT mice. These data indicate that the deficiency of IDH2 promotes melanogenesis pathway.

We observed that the deficiency of IDH2 induces oxidative DNA damage in keratinocytes, thereby leading to the production of α-MSH *in vitro*. The deficiency of IDH2 in mice resulted in an increase in the pigmentation on the dorsal skin. To investigate the role of IDH2 in keratinocytes *in vivo*, we measured the phosphorylation level of γ-H2AX, ATM, Chk2, and p53 signaling pathways with immunohistochemistry. All sections were counterstained with anti-keratin antibody (red) for pan-keratinocytes and Hoechst 33342 (blue) for nuclear morphology. An increase in the intensity of DNA damage markers was observed in skin keratinocytes of KO mice as compared with WT mice. These data show that IDH2 deficiency caused oxidative DNA damage in skin keratinocytes, leading to the secretion of α-MSH and the subsequent enhancement of melanin synthesis in skin melanocytes. To assess the oxidative damage in skin tissue caused by the deficiency of IDH2, we used 8-OH-dG (Fig. 3I). Sections were counterstained with anti-keratin antibody (red) for pan-keratinocytes and Hoechst 33342 (blue) for nuclear morphology. To quantify ROS production in skin keratinocytes, MitoSOX Red was used [51]. Sections were counterstained with anti-keratin antibody (green) for pan-keratinocytes and Hoechst 33342 (blue) for nuclear morphology. We

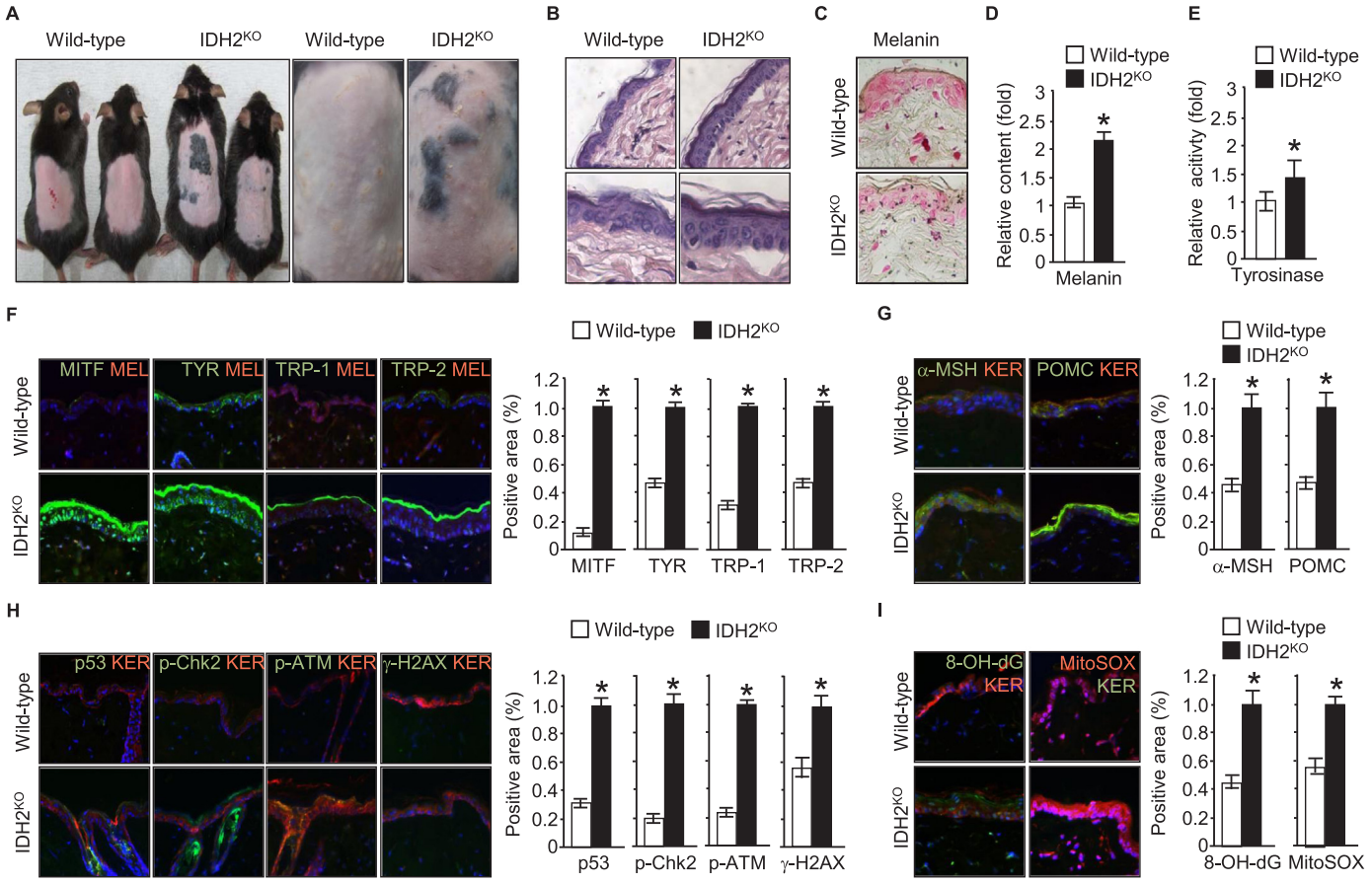

Fig. 3. Effects of IDH2 deficiency on the skin melanogenesis of mice. The dorsal skin of mice (10–12 weeks old) was shaved with a trimmer, followed by their euthanization. (A) Dorsal skin images of WT and *IDH2*$^{-/-}$ KO mice. (B) Hematoxylin & eosin staining for the evaluation of the histological image of WT and KO mice skin. (C) Masson-Fontana staining of the dorsal skin for the analysis of skin melanin content. (D) Melanin content of skin from WT and KO mice. (E) Tyrosinase activity assay was used to detect tyrosinase activity of both WT and KO mice skin. (F) Representative immunohistochemical images of melanin synthesis markers such as MITF, tyrosinase, TRP1, and TRP2 in mice skin. All sections were counterstained with anti-melanoma antibody (red) for pan-melanocytes. Nuclei were counterstained with Hoechst 33342. (G) Immunofluorescence image of α-MSH and POMC in mice skin. All sections were counterstained with anti-pan-keratinocyte antibody (red) for pan-keratinocytes and Hoechst 33342 (blue) for nuclear morphology. (H) Immunofluorescence image of DNA damage markers such as p53, p-Chk2, p-ATM, and γ-H2AX in mice skin. All sections were counterstained with anti-pan-keratinocyte antibody (red) for pan-keratinocytes and Hoechst 33342 (blue) for nuclear morphology. (I) Immunofluorescence image of 8-OH-dG (green) and MitoSOX (red) in mice skin. Sections were stained with pan-keratinocyte and Hoechst 33342 (blue). All histograms represent the quantification of fluorescence intensity. In D-I, results are shown as the mean ± SD (n = 3–6 mice in each group). *$p < 0.05$ between the two genotypes indicated.

observed an increase in the intensity in KO mice as compared with WT mice.

Immunofluorescence images of NADPH, GSSG, and Prx-SO_3 were obtained (Supplementary Fig. 1B). NADPH has a role in the intracellular redox status as a reducing agent in the antioxidant system [52]. NADPH level was reduced in KO mice, as evident from the decrease in the immunofluorescence. GSSG is an oxidized form of GSH and may be used as a parameter to study the intracellular redox status [53]. We measured the level of GSSG with immunohistochemistry and found higher intensity for KO mice as compared with WT mice. In addition, we evaluated the level of oxidized Prx-SO_3 to detect oxidative stress in the dorsal skin tissue and found that Prx-SO_3 level was increased in KO mice. These data indicate that IDH2-deficient mice exhibit higher oxidative stress in skin that leads to skin pigmentation.

3.4. Mito-TEMPO alleviates the increased level of melanogenesis in IDH2-deficient mice

To investigate whether mitochondrial ROS plays a major role in skin melanogenesis *in vivo*, the protective role of mitochondria-targeted antioxidant mito-TEMPO was evaluated. Male C57BL/6 KO mice (6-week old) received a daily intraperitoneal injection of mito-TEMPO (0.7 mg/kg) or vehicle for 30 days. After 30 days, mice dorsal skin was shaved with a trimmer, followed by their euthanization. As shown in Fig. 4A, KO mice showed skin pigmentation, while amelioration of pigmentation was observed in mito-TEMPO-treated mice. As shown in Fig. 4B, H&E-stained dorsal skin sections revealed the difference between KO and mito-TEMPO-treated mice for the integrity of skin layers and thickness. The image indicates that the dorsal skin of KO mice showed thick epidermis layers. Melanin was heavily distributed in the whole layer of the epidermis, including melanocytes and keratinocytes. Masson-Fontana staining was used to examine the deposition of melanin pigments in KO and mito-TEMPO-treated mice (Fig. 4C). An increase in the melanin content was observed in the epidermis layer of skin from KO mice as well as hair follicle to a lesser extent, and mito-TEMPO treatment ameliorated this effect. Furthermore, we measured melanin content (Fig. 4D) and tyrosinase activity (Fig. 4E) and found that the melanin content and tyrosinase activity decreased in the dorsal skin of mito-TEMPO-mice as compared with KO mice. We evaluated the expression level of melanin synthesis markers with immunohistochemistry (Fig. 4F). Sections were counterstained with anti-melanoma antibody (red) for pan-melanocytes and Hoechst 33342 (blue) for nuclear morphology. We found an increase in the intensity of MITF in KO mice as compared with mito-TEMPO-treated mice, as

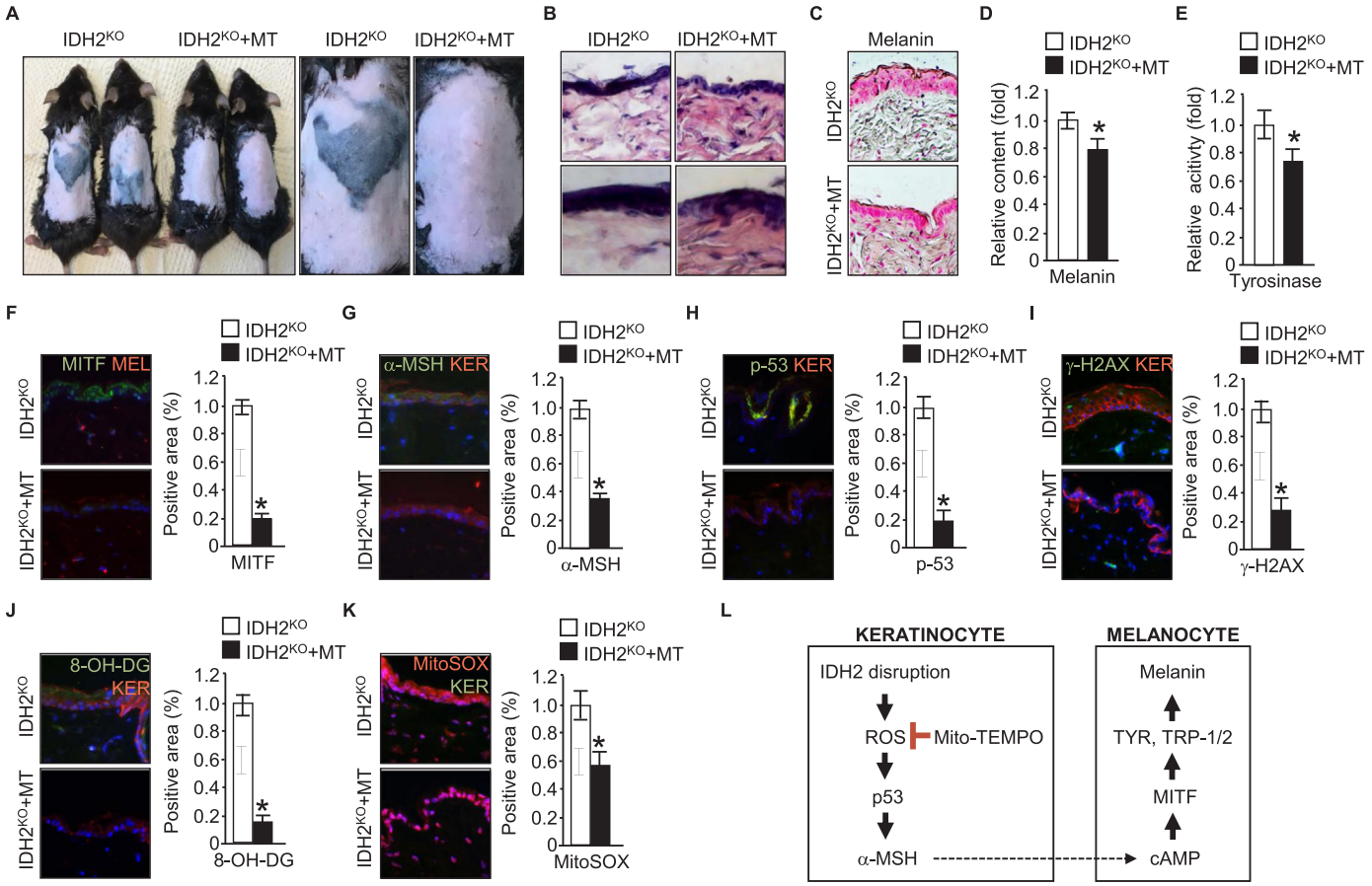

Fig. 4. Mito-TEMPO alleviates the increased level of melanogenesis in IDH2-deficient mice. Male juvenile C57BL/6 mice (6-week old) received a daily injection of mito-TEMPO (0.7 mg/kg, i.p.) for 30 days. (A) Dorsal skin images of untreated KO mice and KO mice treated with mito-TEMPO. (B) Hematoxylin & eosin staining for the evaluation of the histological image. (C) Masson-Fontana staining of skin for the analysis of the melanin content. (D) The melanin content was measured to evaluate melanin production in untreated KO mice and KO mice treated with mito-TEMPO. (E) Tyrosinase activity assay was used to detect tyrosinase activity in mice skin. (F) Immunofluorescence image of mice skin for MITF. Sections were stained with anti-melanoma antibody (red) for pan-melanocytes and Hoechst 33342 for nuclear morphology. (F) Immunofluorescence image of mice skin for α-MSH. (H) Immunofluorescence image of mice skin for p53. (I) Immunofluorescence image of mice skin for γ-H2AX. All sections were counterstained with anti-pan-keratinocyte antibody (red) for pan-keratinocytes and Hoechst 33342 (blue) for nuclear morphology. (J) Immunofluorescence image of mice skin for 8-OH-dG (green). (K) Immunofluorescence image of mice for MitoSOX (red). Sections were stained with pan-keratinocyte and Hoechst 33342 (blue). (L) Schematic diagram summarizing that IDH2 deficiency promotes melanogenesis. In D-I, results are shown as the mean ± SD (n = 3–6 mice in each group). *$p < 0.05$ versus KO mice untreated with mito-TEMPO.

confirmed with immunoblot analysis (Supplementary Fig. 2A). The expression level of representative melanogenesis markers such as MITF, tyrosinase, TRP1, and TRP2 decreased in mito-TEMPO-treated mice as compared with KO mice. Thus, the treatment with mito-TEMPO resulted in the reduction of melanin synthesis signals that were increased in IDH2-deficient skin *in vivo*. We analyzed α-MSH level with immunofluorescence staining to determine whether IDH2 deficiency affects α-MSH level and the effect of mito-TEMPO treatment on α-MSH level (Fig. 4G). The results show that the level of α-MSH decreased in mito-TEMPO-treated mice as compared with KO mice.

We measured the phosphorylation level of γ-H2AX, ATM, Chk2, and p53 in IDH2 KO mice. To determine the effect of mito-TEMPO treatment on oxidative DNA damage in response to IDH2 deficiency, immunofluorescence staining of phosphorylated γ-H2AX and p53 was performed (Figs. 4H and 4I). All sections were counterstained with anti-keratin antibody (red) for pan-keratinocytes and Hoechst 33342 (blue) for nuclear morphology. We observed an increase in the intensity of DNA damage markers in skin keratinocytes of KO mice, while mito-TEMPO-treated mice showed a decrease in the staining intensity. To assess the effects of mito-TEMPO against oxidative damage in response to IDH2 deficiency, we used 8-OH-dG for the quantification of oxidative DNA damage in skin (Fig. 4J). Sections were counterstained with anti-keratin antibody (red) for pan-keratinocytes and Hoechst 33342 (blue) for nuclear morphology. To quantify ROS production in skin keratinocytes, MitoSOX Red was used. Sections were counterstained with anti-pan-keratinocyte antibody (green) for pan-keratinocytes and Hoechst 33342 (blue) for nuclear morphology. An increase in the intensity was observed in KO mice, while the intensity decreased in mito-TEMPO-treated mice (Fig. 4K). To investigate the effect of mito-TEMPO treatment against oxidative stress in response to IDH2 deficiency, immunohistochemistry of GSSG and NADPH was performed. As shown Supplementary Fig. 2B, mito-TEMP treatment abrogated the increase in the intensity of GSSG and recovered the level of NADPH in KO mice. Thus, the oxidative damage in KO mice was alleviated after mito-TEMPO treatment.

In conclusion, the present study shows that IDH2 deficiency leads to increased oxidative DNA damage in keratinocytes and enhances melanin synthesis in melanoma cells and dorsal skin of mice through the disruption of the mitochondrial redox status. Having established the importance of IDH2 in the regulation of the mitochondrial redox status and skin pigmentation, we propose that the downregulation of IDH2 *in vitro* and *in vivo* may serve as an effective strategy for future melanogenesis research. Furthermore, our study provides a useful model to investigate the potential application of mito-TEMPO in the treatment or prevention of skin pigmentation by regulating mitochondrial redox status.

Acknowledgement

This work was supported by the National Research Foundation of Korea (NRF) grant funded by the Korea government (MSIP) (Grant No. NRF-2015R1A4A1042271).

Appendix A. Supporting information

Supplementary data associated with this article can be found in the online version at http://dx.doi.org/10.1016/j.redox.2018.04.008.

References

[1] S.A. D'Mello, G.J. Finlay, B.C. Baguley, M.E. Askarian-Amiri, Signaling pathways in melanogenesis, Int. J. Mol. Sci. 17 (2016) E1144.
[2] P.M. Plonka, T. Passeron, M. Brenner, D.J. Tobin, S. Shibahara, A. Thomas, A. Slominski, A.L. Kadekaro, D. Hershkovitz, E. Peters, J.J. Nordlund, Z. Abdel-Malek, K. Takeda, R. Paus, J.P. Ortonne, V.J. Hearing, K.U. Schallreuter, What are melanocytes really doing all day long…? Exp. Dermatol. 18 (2009) 799–819.
[3] M. Brenner, V.J. Hearing, The protective role of melanin against UV damage in human skin, Photochem. Photobiol. 84 (2008) 539–549.
[4] T. Herrling, K. Jung, J. Fuchs, The role of melanin as protector against free radicals in skin and ints role as free radical indicator in hair, Spectrochim. Acta A Mol. Biomol. Spectrosc. 69 (2008) 1429–1435.
[5] C. Delevoye, Melanin transfer: the keratinocytes are more than gluttons, J. Invest. Dermatol. 134 (2014) 877–879.
[6] M. Cichorek, M. Wachulska, A. Stasiewicz, A. Tymińska, Skin melanocytes: biology and development, Postepy Dermatol. Alergol. 30 (2013) 30–41.
[7] Y.H. Shin, Y.K. Seo, H.H. Yoon, K.Y. Song, J.K. Park, Effect of keratinocytes on regulation of melanogenesis in culture of melanocytes, Biotechnol. Bioprocess. Eng. 17 (2012) 203–210.
[8] D.J. Tobin, The cell biology of human hair follicle pigmentation, Pigment Cell Melanoma Res. 24 (2011) 75–88.
[9] A. Slominski, J. Wortsman, P.M. Plonka, K.U. Schallreuter, R. Paus, D.J. Tobin, Hair follicle pigmentation, J. Investig. Dermatol. 124 (2005) 13–21.
[10] M. Oren, J. Bartek, The sunny side ofp53, Cell 128 (2007) 826–828.
[11] S. Shibahara, K. Takeda, K.I. Yasumoto, T. Udono, K.I. Watanabe, H. Saito, K. Takahashi, Microphthalmia-associated transcription factor (MITF): multiplicity in structure, function, and regulation, J. Investig. Dermatol. Symp. Proc. 6 (2001) 99–104.
[12] P.C. Eves, S. MacNeil, J.W. Haycock, alpha-Melanocyte stimulating hormone, inflammation and human melanoma, Peptides 27 (2006) 444–452.
[13] Y. Yamaguchi, M. Brenner, V.J. Hearing, The regulation of skin pigmentation, J. Biol. Chem. 282 (2007) 27557–27561.
[14] A.J. Nappi, E. Vass, Hydrogen peroxide generation associated with the oxidations of the eumelanin precursors 5, 6-dihydroxyindole and 5, 6-dihydroxyindole-2-carboxylic acid, Melanoma Res. 6 (1996) 341–349.
[15] E.S. Cunha, R. Kawahara, M.K. Kadowaki, H.G. Amstalden, G.R. Noleto, S.M. Cadena, S.M. Winnischofer, G.R. Martinez, Melanogenesis stimulation in B16-F10 melanoma cells induces cell cycle alterations, increased ROS levels and a differential expression of proteins as revealed by proteomic analysis, Exp. Cell Res. 318 (2012) 1913–1925.
[16] N.C. Jenkins, D. Grossman, Role of melanin in melanocyte dysregulation of reactive oxygen species, Biomed. Res. Int. (2013) 908797.
[17] W. Ding, L.G. Hudson, K.J. Liu, Inorganic arsenic compounds cause oxidative damage to DNA and protein by inducing ROS and RNS generation in human keratinocytes, Mol. Cell. Biochem. 279 (2005) 105–112.
[18] E. Pelle, T. Mammone, D. Maes, K. Frenkel, Keratinocytes act as a source of reactive oxygen species by transferring hydrogen peroxide to melanocytes, J. Investig. Dermatol. 124 (2005) 793–797.
[19] H.C. Huang, W.Y. Hsieh, Y.L. Niu, T.M. Chang, Inhibition of melanogenesis and antioxidant properties of *Magnolia grandiflora* L. flower extract, BMC Complement. Altern. Med. 12 (2012) 72.
[20] C. Quan, M.K. Cho, D. Perry, T. Quan, Age-associated reduction of cell spreading induces mitochondrial DNA common deletion by oxidative stress in human skin dermal fibroblasts: implication for human skin connective tissue aging, J. Biomed. Sci. 22 (2015) 62.
[21] G. Wu, Y.Z. Fang, S. Yang, J.R. Lupton, N.D. Turner, Glutathione metabolism and its implications for health, J. Nutr. 134 (2004) 489–492.
[22] L. Moldovan, N.I. Moldovan, Oxygen free radicals and redox biology of organelles, Histochem. Cell Biol. 122 (2004) 395–412.
[23] H. Esterbauer, R.J. Schaur, H. Zollner, Chemistry and biochemistry of 4-hydroxynonenal, malonaldehyde and related aldehydes, Free Radic. Biol. Med. 11 (1991) 81–128.
[24] A.P. Vivancos, E.A. Castillo, B. Biteau, C. Nicot, J. Ayté, M.B. Toledano, E. Hidalgo, A cysteine-sulfinic acid in peroxiredoxin regulates H_2O_2-sensing by the antioxidant Pap1 pathway, Proc. Natl. Acad. Sci. USA 102 (2005) 8875–8880.
[25] T. Wei, C. Chen, J. Hou, J. Xin, A. Mori, Nitric oxide induces oxidative stress and apoptosis in neuronal cells, Biochim. Biophys. Acta 1498 (2000) 72–79.
[26] G.R. Rosania, Mitochondria give cells a tan, Chem. Biol. 12 (2005) 412–413.
[27] L. Ni-Komatsu, S.J. Orlow, Identification of novel pigmentation modulators by chemical genetic screening, J. Investig. Dermatol. 127 (2007) 1585–1592.
[28] T. Daniele, I. Hurbain, R. Vago, G. Casari, G. Raposo, C. Tacchetti, M.V. Schiaffino, Mitochondria and melanosomes establish physical contacts modulated by Mfn2 and involved in organelle biogenesis, Curr. Biol. 24 (2014) 393–403.
[29] J.H. Lee, S.Y. Kim, I.S. Kil, J.-W. Park, Regulation of ionizing radiation-induced apoptosis by mitochondrial $NADP^+$-dependent isocitrate dehydrogenase, J. Biol. Chem. 282 (2007) 13385–13394.
[30] S.H. Jo, M.K. Son, H.J. Koh, S.M. Lee, I.H. Song, Y.O. Kim, Y.S. Lee, K.S. Jeong, W.B. Kim, J.-W. Park, B.J. Song, T.L. Huh, Control of mitochondrial redox balance and cellular defense against oxidative damage by mitochondrial $NADP^+$-dependent isocitrate dehydrogenase, J. Biol. Chem. 276 (2001) 16168–16176.
[31] H.J. Ku, Y. Ahn, J.H. Lee, K.M. Park, J.-W. Park, IDH2 deficiency promotes mitochondrial dysfunction and cardiac hypertrophy in mice, Free Radic. Biol. Med. 80 (2015) 84–92.
[32] J.H. Park, H.J. Ku, J.H. Lee, J.-W. Park, *Idh2* deficiency exacerbates acrolein-induced lung injury through mitochondrial redox environment deterioration, Oxid. Med. Cell. Longev. (2017) 1595103.
[33] B.I. Ratnikov, D.A. Scott, A.L. Osterman, J.W. Smith, Z.E.A. Ronai, Metabolic rewiring in melanoma, Oncogene 36 (2017) 147.
[34] H. Guo, K. Yang, F. Deng, Y. Xing, Y. Li, X. Lian, T. Yang, Wnt3a inhibits proliferation but promotes melanogenesis of melan-a cells, Int. J. Mol. Med. 30 (2012) 636–642.
[35] R. Ni, T. Cao, S. Xiong, J. Ma, G.C. Fan, J.C. Lacefield, Y. Lu, S. Le Tissier, T. Peng, Therapeutic inhibition of mitochondrial reactive oxygen species with mito-TEMPO reduces diabetic cardiomyopathy, Free Radic. Biol. Med. 90 (2016) 12–23.
[36] J.G. Pastorino, G. Simbula, K. Yamamoto, P.A. Glascott, R.J. Rothman, J.L. Farber, The cytotoxicity of tumor necrosis factor depends on induction of the mitochondrial permeability transition, J. Biol. Chem. 271 (1996) 29792–29798.
[37] H.S. Jang, J.I. Kim, K.J. Jung, J. Kim, K.H. Han, K.M. Park, Bone marrow-derived cells play a major role in kidney fibrosis via proliferation and differentiation in the infiltrated site, Biochim. Biophys. Acta 2013 (1832) 817–825.
[38] J. Bartek, J. Lukas, Chk1 and Chk2 kinases in checkpoint control and cancer, Cancer Cell 3 (2003) 421–429.
[39] M.B. Kastan, J. Bartek, Cell-cycle checkpoints and cancer, Nature 432 (2004) 316–323.
[40] H.C. Reinhardt, B. Schumacher, The p53 network: cellular and systemic DNA damage responses in aging and cancer, Trends Genet. 28 (2012) 128–136.
[41] L.J. Kuo, L.X. Yang, γ-H2AX-a novel biomarker for DNA double-strand breaks, In vivo 22 (2008) 305–309.
[42] A. Slominski, D. Heasley, J.E. Mazurkiewicz, G. Ermak, J. Baker, J.A. Carlson, Expression of proopiomelanocortin (POMC)-derived melanocyte-stimulating hormone (MSH) and adrenocorticotropic hormone (ACTH) peptides in skin of basal cell carcinoma patients, Hum. Pathol. 30 (1999) 208–215.
[43] H. Kasai, Analysis of a form of oxidative DNA damage, 8-hydroxy-2′-deoxyguanosine, as a marker of cellular oxidative stress during carcinogenesis, Mutat. Res. 387 (1997) 147–163.
[44] J. Han, L.A. Goldstein, W. Hou, C.J. Froelich, S.C. Watkins, H. Rabinowich, Deregulation of mitochondrial membrane potential by mitochondrial insertion of granzyme B and direct Hax-1 cleavage, J. Biol. Chem. 285 (2010) 22461–22472.
[45] J.J. Lemasters, A.L. Nieminen, T. Qian, L.C. Trost, S.P. Elmore, S.P. Nishimura, R.A. Crowe, W.E. Cascio, C.A. Bradham, D.A. Brenner, B. Herman, The mitochondrial permeability transition in cell death: a common mechanism in necrosis, apoptosis and autophagy, Biochim. Biophys. Acta 1366 (1998) 177–196.
[46] I.F.D.S. Videira, D.F.L. Moura, S. Magina, Mechanisms regulating melanogenesis, An. Bras. Dermatol. 88 (2013) 76–83.
[47] A.E. Dikalova, A.T. Bikineyeva, K. Budzyn, R.R. Nazarewicz, L. McCann, W. Lewis, D.G. Harrison, S.I. Dikalov, Therapeutic targeting of mitochondrial superoxide in hypertension, Circ. Res 107 (2010) 106–116.
[48] H.L. Liang, F. Sedlic, Z. Bosnjak, V. Nilakantan, SOD1 and mito-TEMPO partially prevent mitochondrial permeability transition pore opening, necrosis, and mitochondrial apoptosis after ATP depletion recovery, Free Radic. Biol. Med. 49 (2010) 1550–1560.
[49] M. Liu, H. Liu, S.C. Dudley, Reactive oxygen species originating from mitochondria regulate the cardiac sodium channel, Circ. Res. 107 (2010) 967–974.
[50] R. Cui, H.R. Widlund, E. Feige, J.Y. Lin, D.L. Wilensky, V.E. Igras, J. D'Orazio, C.Y. Fung, C.F. Schanbacher, S.R. Granter, D.E. Fisher, Central role of p53 in the suntan response and pathologic hyperpigmentation, Cell 128 (2007) 853–864.
[51] L. Valls-Lacalle, I. Barba, E. Miró-Casas, J.J. Alburquerque-Béjar, M. Ruiz-Meana, M. Fuertes-Agudo, A. Rodríguez-Sinovas, D. García-Dorado, Succinate dehydrogenase inhibition with malonate during reperfusion reduces infarct size by preventing mitochondrial permeability transition, Cardiovasc. Res. 109 (2015) 374–384.
[52] M. Kirsch, H. de Groot, NAD(P)H, a directly operating antioxidant? FASEB J. 15 (2001) 1569–1574.
[53] S. Bharath, M. Hsu, D. Kaur, S. Rajagopalan, J.K. Andersen, Glutathione, iron and Parkinson's disease, Biochem. Pharmacol. 64 (2002) 1037–1048.